Inorganic Chemistry

Article

pubs.acs.org/IC

Oxygen Kinetic Isotope Effects upon Catalytic Water Oxidation by a Monomeric Ruthenium Complex

Alfredo M. Angeles-Boza and Justine P. Roth*

Department of Chemistry, Johns Hopkins University, 3400 North Charles Street, Baltimore, Maryland 21218, United States

Supporting Information

ABSTRACT: Oxygen isotope fractionation is applied for the first time to probe the catalytic oxidation of water using a widely studied ruthenium complex, $[Ru^{II}(tpy)(bpy)(H_2O)](ClO_4)_2$ (bpy = 2,2′-bipyridine; tpy = 2,2′;6″,2″-terpyridine). Competitive oxygen-18 kinetic isotope effects (^{18}O KIEs) derived from the ratio of $^{16,16}O_2$ to $^{16,18}O_2$ formed from natural-abundance water vary from 1.0132 ± 0.0005 to 1.0312 ± 0.0004. Experiments were conducted with cerium(IV) salts at low pH and a photogenerated ruthenium(III) tris(bipyridine) complex at neutral pH as the oxidants. The results are interpreted within the context of catalytic mechanisms using an adiabatic formalism to ensure the highest barriers for electron-transfer and proton-coupled electron-transfer steps. In view of these contributions, O−O bond formation is predicted to be irreversible and turnover-limiting. The reaction with the largest ^{18}O KIE exhibits the greatest degree of O−O coupling in the transition state. Smaller ^{18}O KIEs are observed due to multiple rate-limiting steps or transition-state structures which do not involve significant O−O motion. These findings provide benchmarks for systematizing mechanisms of O−O bond formation, the critical step in water oxidation by natural and synthetic catalysts. In addition, the measurements introduce a new tool for calibrating computational studies using relevant experimental data.

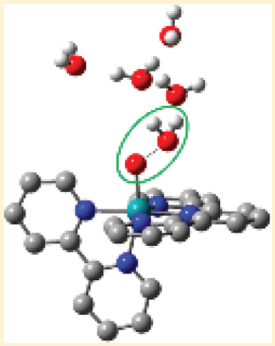

INTRODUCTION

Progress toward establishing a hydrogen economy[1] requires a greater fundamental understanding of how water is oxidized to molecular oxygen.[2] Although inorganic entities capable of the catalytic transformation in Figure 1 have been sought after and studied for a number of years, the mechanisms of O−O bond coupling, particularly within mononuclear ruthenium complexes, remain obscure.[3] Reported here as new mechanistic probes are measurements of competitive oxygen-18 kinetic isotope effects (^{18}O KIEs) under various experimental conditions. All results reveal more $^{16,16}O_2$ is formed than $^{16,18}O_2$ from natural-abundance water, indicating moderate-to-large normal ^{18}O KIEs.

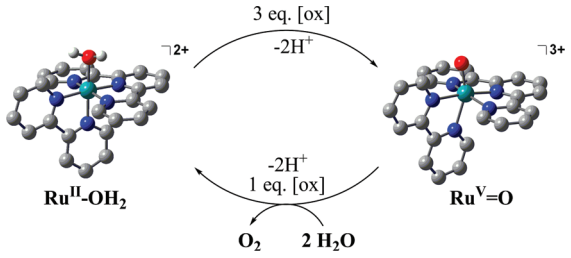

Figure 1. Generally proposed mechanism for water oxidation by a single-site ruthenium catalyst.[3]

Monomeric ruthenium polypyridyl complexes that bind H_2O may undergo chemical oxidation by ceric (Ce^{IV}) ions at low pH[4−12] and by oxidants like $[Ru(bpy)_3]^{3+}$ at neutral pH in the presence of a proton acceptor.[13] Although the oxidation state formalism for the reactive ruthenyl intermediate has been questioned, the species depicted above as $[Ru^{V}{=}O]^{3+}$ has a greater reduction potential than the $[Ru^{IV}{=}O]^{2+}$ precursor and is more generally implicated in mechanisms of single-site catalysts.[3]

On the basis of isotope tracer studies, O_2 is known to originate from the aqueous solvent, which undergoes rapid reversible exchange with $[\mathbf{Ru^{II}OH_2}]^{2+}$.[14] As in Figure 1, the solvent H_2O nucleophilically attacks the transient $[Ru^{V}{=}O]^{3+}$, forming an O−O bond that is retained within the hydroperoxo intermediate, $[Ru^{III}OOH_2]^{3+}$, or its deprotonated form, $[Ru^{III}OOH]^{2+}$. This species is oxidized to a dioxygen adduct, formally $Ru^{III}O_2^{I-}$ or $Ru^{IV}O_2^{II-}$, which spontaneously releases O_2 concomitant with or before coordination of a second H_2O.

Beginning with $[\mathbf{Ru^{II}OH_2}]^{2+}$, a single-turnover reaction is shown in Figure 2 (eqs 1−6). Experiments in this study using substoichiometric levels of oxidant have confirmed that 1 equiv of O_2 is evolved every time 4 equiv of oxidant [ox] and base [B:] are consumed. In contrast, 5 oxidizing equiv would be required for an alternate single-turnover pathway, where H_2O_2 is released from the catalyst by protonolysis before being converted to O_2 by (eqs 7 and 8) and recycling the Ru^{III} form of the catalyst.

$[Ru^{II}(tpy)(bpy)(H_2O)](ClO_4)_2$ (bpy = 2,2′-bipyridine; tpy = 2,2′;6″,2″-terpyridine), referred to in Figure 1 as $[\mathbf{Ru^{II}OH_2}]^{2+}$, was synthesized in pure form.[15] ***Caution!*** *Perchlorate salts are potentially explosive.* The complex has been thoroughly studied

Received: December 22, 2011
Published: March 30, 2012

   dx.doi.org/10.1021/ic202745n | Inorg. Chem. 2012, 51, 4722−4729

(1) $[Ru^{II}\text{-}OH_2]^{2+} + [ox] + n[B:] \underset{k_{-1}}{\overset{k_1}{\rightleftharpoons}} [Ru^{III}\text{-}OH_{2-n}]^{2+} + [red] + n[BH^+]$

(2) $[Ru^{III}\text{-}OH_{2-n}]^{2+} + [ox] + 2\text{-}n[B:] \underset{k_{-2}}{\overset{k_2}{\rightleftharpoons}} [Ru^{IV}{=}O]^{2+} + [red] + 2\text{-}n[BH^+]$

(3) $[Ru^{IV}{=}O]^{2+} + [ox] \underset{k_{-3}}{\overset{k_3}{\rightleftharpoons}} [Ru^{V}{=}O]^{3+} + [red]$

(4) $[Ru^{V}{=}O]^{3+} + H_2O + [B:] \underset{k_{-4}}{\overset{k_4}{\rightleftharpoons}} [Ru^{III}\text{-}OOH]^{2+} + [BH^+]$

(5) $[Ru^{III}\text{-}OOH]^{2+} + [ox] + [B:] \xrightarrow{k_5} [Ru^{III}\text{-}O_2]^{2+} + [red] + [BH^+]$

(6) $[Ru^{III}\text{-}O_2]^{2+} + H_2O \xrightarrow{k_6} [Ru^{II}\text{-}OH_2]^{2+} + O_2$

(7) $[Ru^{III}\text{-}OOH]^{2+} + H_2O \xrightarrow{k_7} [Ru^{III}\text{-}OH]^{2+} + H_2O_2$

(8) $H_2O_2 + 2[ox] + 2[B:] \xrightarrow{k_8} O_2 + 2[red] + 2[BH^+]$

Figure 2. Reactions culminating in water oxidation: n = 0 at low pH and n = 1 at neutral pH.

and may be regarded as a prototypical single-site catalyst, exhibiting moderate stability and turnover numbers (TONs) that make it ideal for the present investigations.[5] The isotope fractionation method[16] used to obtain competitive ^{18}O KIEs upon reactions in Figure 3 is analogous to that applied in earlier

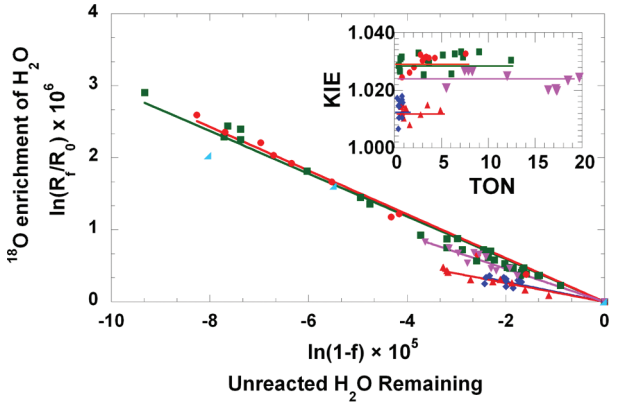

Figure 3. Oxygen isotope fractionation during water oxidation. Solutions contained $[\mathbf{Ru^{II}OH_2}]^{2+}$ and the following oxidants: CAN in 1.0 M $HClO_4$ (orange circles), CAN in 0.1 M $HClO_4$ (green squares), CAN in 1.0 M HNO_3 (cyan right triangles), CS in 1.0 M HNO_3 (lilac inverted triangles), CS in 0.1 M $HClO_4$ (red triangles), and $Ru^{III}(bpy)_3^{3+}$ in 0.05 M KPi buffered to pH 7.2 (blue diamonds). Inset: ^{18}O KIE versus catalyst TON at 22 °C.

studies of water oxidation during photosynthesis. The resultant ^{18}O KIEs serve as probes of O−O bond-forming mechanisms. For this reason, we chose to evaluate ^{18}O KIEs upon reactions of the same catalyst in acidic and neutral media with different sacrificial oxidants, where the kinetic contribution from O−O bond coupling may vary.

The ^{18}O KIEs are interpreted using a wealth of published data[4−9,11] to predict reaction coordinates for water oxidation. Standard electrochemical potentials ($E°'$) are quoted versus the normal hydrogen electrode (NHE) for each electron transfer (ET) and concerted proton-coupled electron transfer (PCET).[17] While steady-state kinetics at low pH and the associated ^{18}O KIEs are the focus of this study, previously published results[5−9] reflect pre-steady-state rate constants corresponding to eqs 1−6 in Figure 2, together with a steady-state rate constant quoted for O_2 evolution (at what appears to be saturating CAN concentrations).[6] Analyses of ET and PCET are performed within the adiabatic limit to give upper bounds to activation free-energy barriers ($\Delta G^{‡}$). Although nonadiabatic formalisms can offer more nuanced quantum-mechanical descriptions of such reactions,[17] the objective of this study is to maximize barriers so as to conservatively compare $\Delta G^{‡}$ for ET and PCET steps to the $\Delta G^{‡}$ for O−O coupling and O_2 evolution.

EXPERIMENTAL SECTION

Preparation of Compounds. All chemicals were purchased commercially in the highest purity available and used as received. $RuCl_3 \cdot nH_2O$ was obtained from Pressure Chemicals. Perchloric acid (70%), nitric acid (70%), and potassium phosphate buffers were obtained from Fisher Scientific. Ceric ammonium nitrate (CAN), ceric sulfate tetrahydrate (CS), a standardized 1 M ceric sulfate solution, 2,2′-bipyridine (bpy), 2,2′;6′,2″-terpyridine (tpy), $K_2S_2O_8$, KNO_3, $LiClO_4$, and $Ru(bpy)_3Cl_2$ were purchased from Sigma-Aldrich. Riedel-de Haën provided an additional source of CS. Hexamethyldisiloxane (HMDS) was obtained from Lancaster and MeOD-d_3 acquired from Cambridge Isotope Laboratories.

$[Ru(tpy)(bpy)(H_2O)](ClO_4)_2$ ($[\mathbf{Ru^{II}OH_2}]^{2+}$) was synthesized according to a reported procedure[7] ***Caution!*** *Perchlorate salts can be explosive and should be handled with care.* The analytical purity of $[\mathbf{Ru^{II}OH_2}]^{2+}$ was confirmed by elemental analysis (Atlantic Microlabs, Norcross, GA), which gave the following results. Calcd: C, 42.44; H, 2.99; N, 9.90. Found: C, 42.16; H, 2.76; N, 9.77. A comparison to the reported extinction coefficient of $\varepsilon_{475\ nm}$ (9600 M^{-1} cm^{-1}) using a Beer's law plot indicated $\varepsilon_{475\ nm}$ = 9000 ± 150 $M^{-1}cm^{-1}$.[15] Thus, multiple samples of $[\mathbf{Ru^{II}OH_2}]^{2+}$ used in the analysis were judged to be of at least 94 ± 6% purity, consistent with ^1H NMR measurements carried out on a 400 MHz Bruker Avance spectrometer at ambient temperature. The NMR sample contained 1.3 × 10^{-5} mol of $[\mathbf{Ru^{II}OH_2}]^{2+}$ and 1.2 × 10^{-5} mol of HMDS in CD_3OD. Chemical shifts were referenced to the residual protio impurities in the deuterated solvent. The purity of this sample based on integration versus the HMDS internal standard was 99 ± 6%.[15] Water used in all experiments was purified to 18 MΩ by passing through a Millipore ultrafiltration system.

Physical Methods. Electronic absorption spectra were recorded on a diode-array UV−vis spectrophotometer (Agilent 8453). Rates of O_2 evolution were measured using a Clark-type oxygen electrode (Yellow Springs Inc.; 5300A voltmeter and 5331A probe). A custom-built mixing chamber was used to maintain the solution temperature at 22 ± 0.2 °C with a recirculating water bath (VWR). The O_2 concentration versus time was monitored after initiation by injecting solutions of $[\mathbf{Ru^{II}OH_2}]^{2+}$ or Ce^{IV} into a stirring solution. Cyclic voltammetry experiments were recorded on a BASF electrochemical analyzer using methods described previously.[6]

Preparation of Water Samples for Isotopic Analysis. The ratio of $^{18}O/^{16}O$ in unreacted natural-abundance water is designated R_0. These samples were taken directly from the Millipore filtration unit. In some cases, the water was isolated by the vacuum transfer of all volatiles from solutions of 0.1 M $HClO_4$. R_0 was also determined for samples of 0.1 M $HClO_4$ preincubated for 20 min with the reduced metal catalyst (600 μM) or CAN (0.05 M) before vacuum transfer of the liquid into glass ampules, which were then flame-sealed. A standard CO_2 exchange protocol was used for analysis of H_2O and consistently indicated R_0 = 0.9930 ± 0.0006 versus Vienna Standard Mean Ocean Water (VSMOW). In addition, analyses were conducted at two different isotope ratio mass spectrometry (IRMS) facilities at the University of Waterloo in the Environmental Isotope Laboratory and at Johns Hopkins University in the Department of Earth and Planetary Sciences.

Description of the Competitive ^{18}O KIE upon Photocatalytic Water Oxidation. Following a protocol outlined by Cape et al.,[18] a solution of $Ru(bpy)_3Cl_2$ (225 μM) and $K_2S_2O_8$ (0.015 M) in KPi (0.05 M) was saturated with helium gas at ambient temperature. A 15

dx.doi.org/10.1021/ic202745n | Inorg. Chem. 2012, 51, 4722−4729

mL sample of this neutral solution was then transferred to a quartz bubbler to dissolve the solid sample of $[\mathbf{Ru^{II}OH_2}]^{2+}$. Photolysis was then initiated near 450 nm using a 150-W Hg/Xe lamp (Oriel model 66001) equipped with a dichroic mirror (Spectraphysics 66218). The photolysis experiments were conducted at 22 ± 2 °C under vacuum and helium sparge with constant stirring for 20 min. The O_2 evolved was isolated and purified prior to complete combustion to CO_2, as described in the Results section. Control experiments with all solution components present except for $[\mathbf{Ru^{II}OH_2}]^{2+}$ or $[Ru(bpy)_3]Cl_2$ did not produce detectable levels of O_2.

RESULTS

Sacrificial oxidants used in the following studies were obtained in the highest purity available (≥99%) and reproducibility confirmed among multiple preparations. ^{18}O KIEs and steady-state rate constants were determined for oxidations by CAN and CS at low pH. ^{18}O KIEs were also determined for oxidations by $[Ru^{III}(bpy)_3]^{3+}$ at neutral pH, following an established photogeneration method.[18] While CAN in aqueous $HClO_4$ exhibits $E^{o\prime}$ = 1.57 V at pH 0 and 1.42 V at pH 1,[6] $[Ru^{III}(bpy)_3]^{3+}$ exhibits a pH-independent $E^{o\prime}$ = 1.24 V. Although solutions of CAN may contain $[Ce^{IV}(NO_3)_6]^{2-}$ in a dodecahedral geometry and CS solutions may contain the eight-coordinate $Ce^{IV}(SO_4)_2(H_2O)_4$, the exact identities of the oxidants in strong acids with noncoordinating counterions are questionable and Ce^{IV}–OH species may exist depending on the pH.[19]

Generally, lanthanide complexes exhibit slow electron self-exchange rates because of compromised interactions of the f orbitals and Franck–Condon overlap factors.[20] To the contrary, $[Ru^{III}(bpy)_3]^{3+}$ is one of the fastest-reacting outer-sphere ET reagents, with a bimolecular self-exchange rate constant approaching the diffusion limit.[21] Although $[Ru^{III}(bpy)_3]^{3+}$ can be isolated in pure form,[18b] the complex is short-lived in a potassium phosphate (KPi) buffer at pH 7.2 and, therefore, exhaustive photolysis of $[Ru^{II}(bpy)_3]Cl_2$ in the presence of $K_2S_2O_8$ was used to continuously generate $[Ru^{III}(bpy)_3]^{3+}$. The same oxidant/base combination $[Ru^{III}(bpy)_3]^{3+}/HPO_4^{2-}$ has been used to demonstrate tyrosine oxidation by a mechanism of multisite PCET.[22,23]

The apparatus and methodology used to determine natural-abundance ^{18}O KIEs have been described previously and can easily be constructed in a contemporary inorganic laboratory.[16,24,25] Multiple plant biologists have attempted to use this approach to investigate how O_2 forms as a result of catalytic water oxidation in photosystem II (PSII). This multimeric protein complex utilizes visible photons to generate a catalytically active tyrosyl radical, which is responsible for "water splitting".[26−30] Unfortunately, the ^{18}O KIEs that occur during photosynthetic water oxidation in whole cells and cell fractions have been difficult to measure reproducibly because they are masked by O_2-consuming reactions with reductants present within PSII.[26,27]

Under certain conditions examined, ^{18}O fractionation has given rise to unrealistic isotope effects of ∼0.900.[28] A more reasonable value of 0.990 has also been reported.[29] Some years later, the use of spinach thylakoids, which lack the Mehler reactions of whole cells, resulted in a significantly smaller ^{18}O KIE = 0.9996 ± 0.0003, which only borders on being inverse.[30]

The reasons for the variations in ^{18}O KIEs upon photosynthetic water oxidation have not been understood. Evidence points to unchecked reductive processes that deplete some of the O_2 produced within PSII. A normal ^{18}O KIE, where $^{16,16}O_2$ is consumed preferentially to $^{16,18}O_2$, would lead to a diminution of the normal ^{18}O KIE upon water oxidation because it is O_2 that is analyzed, albeit indirectly. Interferences from O_2 reduction are quite low in spinach thylakoids, where the least inverse ^{18}O KIE has been measured.[30] It is important to realize that if the ^{18}O KIE upon water oxidation were actually inverse, competing ^{18}O enrichments caused by normal ^{18}O KIEs upon O_2 reductions, would make the apparent isotope effect even more inverse. It follows that a competing O_2 reductive process makes the inverse ^{18}O KIEs upon water oxidation appear more inverse, while the normal ^{18}O KIEs upon water oxidation appear "less normal", i.e., closer to unity. Clearly defined water oxidations, which do not suffer from unchecked O_2 reductions, are needed to provide benchmark isotope effects for a wide variety of O–O bond-forming mechanisms, not just those limited to PSII.

The ^{18}O KIEs in this report focus upon a structurally defined ruthenium complex, with well-known kinetic and thermodynamic properties. Most ^{18}O isotope fractionation experiments were conducted by introducing $[\mathbf{Ru^{II}OH_2}]^{2+}$ (cf. Figure 1) into a sealed reaction vessel containing a rapidly stirring, helium-saturated, aqueous solution of the sacrificial oxidant at 22 °C. A fixed-volume aliquot was removed from the collapsible reaction vessel and manipulated in vacuo while purging the sample with helium under dynamic vacuum for 20 min. The O_2 entrained in the helium carrier gas was passed through an additional series of cold traps to remove the less volatile components (e.g., H_2O and CO_2) prior to the collection of pure O_2 on 5 Å molecular sieves at −196 °C.

After helium removal, O_2 was released from the molecular sieves by heating to ∼100 °C. The gas was then quantitatively combusted to CO_2 following an established procedure.[16,30] Pressures were determined using a calibrated capacitance manometer to relate the moles of CO_2 to the moles of O_2 formed from two moles of H_2O. The quantitative nature of the combustion makes the isotope composition of CO_2 identical to the O_2, from which it derived. The CO_2 samples were flamed sealed in dry glass tubes for analysis by dual-inlet IRMS, which gives the $^{18}O/^{16}O$ in a sample versus the analogous ratio in a standard of known composition.

The experimental procedure described above was varied in order to evaluate the reproducibility of the ^{18}O KIEs. In addition to sample contamination, deviant results could occur because of catalyst decomposition or branching of reaction pathways. Certain experiments were initiated by adding a fixed volume of a helium-saturated acidic solution (∼15 mL) to dissolve $[\mathbf{Ru^{II}OH_2}]^{2+}$ along with an excess of CAN or CS, in a glass bubbler (∼300 mL) at a pressure of 20 mTorr. Other experiments were initiated by adding CAN or CS, dissolved in helium-saturated $HClO_4$ or HNO_3, to solid $[\mathbf{Ru^{II}OH_2}]^{2+}$ also under reduced pressure. A slightly different protocol was implemented to photogenerate $[Ru^{III}(bpy)_3]^{3+}$ in a quartz bubbler containing 0.05 M KPi and $[\mathbf{Ru^{II}OH_2}]^{2+}$ together at pH 7.2. During irradiation, the solution maintained at 22 °C was swept with helium under dynamic vacuum to collect the O_2 produced.[15] No O_2 was detected in control experiments, where $[\mathbf{Ru^{II}OH_2}]^{2+}$ was absent and all other conditions remained the same.

The ^{18}O KIEs were analyzed using two approaches that differ with respect to consideration of the fractional conversions. In the first approach, eq 9 was used to approximate the ^{18}O KIE from the $^{18}O/^{16}O$ of the unreacted H_2O (R_0) relative to the $^{18}O/^{16}O$ of the O_2 produced (R_P). R_0 was determined using an established CO_2 equilibration procedure[31] and found to be

dx.doi.org/10.1021/ic202745n | Inorg. Chem. 2012, 51, 4722−4729

Table 1. Reduction Potentials, Rate Constants, and ^{18}O KIEs upon Catalyzed Water Oxidation at 22 °C

conditions[a]	$E^{\circ\prime}$ (V)[b]	k_{un}[c]	μ (M)	k_{con}[c]	μ (M)	KIE[d]	KIE[e]
CAN (1.0 M $HClO_4$)	1.57	0.81 ± 0.11 M^{-1} s^{-1}	1.2−1.5	0.95 ± 0.22 M^{-1} s^{-1}	1.5	1.0299(28)	1.0312(4)
CAN (1.0 M HNO_3)	1.57	0.95 ± 0.06 M^{-1} s^{-1}	1.0−1.1	0.91 ± 0.30 M^{-1} s^{-1}	1.5	1.0281(30)	∼1.0273
CS (1.0 M HNO_3)	∼1.6	0.52 ± 0.16 M^{-1} s^{-1}	1.0−1.1	0.61 ± 0.10 M^{-1} s^{-1}	1.5	1.0233(27)	1.0235(7)
CAN (0.1 M $HClO_4$)	1.42	0.71 ± 0.08 M^{-2} s^{-1}	0.16−0.70	2.31 ± 0.52 M^{-2} s^{-1}	1.0	1.0279(37)	1.0306(4)
CS (0.1 M $HClO_4$)	∼1.6[f]	2.18 ± 0.10 M^{-2} s^{-1}	0.16−0.28	2.45 ± 0.15 M^{-2} s^{-1}	0.30	1.0126(23)	1.0132(5)
$[Ru(bpy)_3]^{3+}$ (0.05 M KPi, pH 7.2)	1.24[g]					1.0143(28)	1.0141(8)

[a]Ionic strengths used to determined ^{18}O KIEs ranged from μ = 0.15 to 1.3 M. [b]From ref 6 (±25−50 mV) unless indicated. [c]k_{un} and k_{con} correspond to rate constants at uncontrolled and controlled ionic strengths. μ in the column to the right specifies the ionic strength ranges. [d]Average ^{18}O KIEs derived from eq 9 and quoted with ±1 standard deviation. [e]Each KIE was fitted to a linearized form of eq 10 (±1 standard error). [f]Measured as described in ref 6. [g]At pH 7.2, $\Delta G^{\circ} = -95.7$ kcal mol^{-1} for PCET. This calculation considers the pK_a (7.2) of HPO_4^{2-} as well as the $E^{\circ\prime}$ of the oxidant.

0.9930 ± 0.0006 relative to VSMOW.[32] R_0 and its error reflect measurements at separate IRMS facilities on independent samples. As expected, because of the large dilution factor, R_0 determined with prepurified 18 MΩ (Millipore) water was indistinguishable from that preincubated with $HClO_4$, CAN, or $[\mathbf{Ru^{II}OH_2}]^{2+}$ at concentrations of 1.0 M, 0.1 M, and ≤1 mM, respectively.

$$^{18}O\ KIE \cong R_0/R_p \tag{9}$$

In contrast to treating H_2O as an "infinite reservoir",[33] the ^{18}O KIE was also determined using eq 10.[15,16] In this treatment, the ^{18}O content of H_2O is calculated in response to the yield of O_2 produced. Although the change in the isotopic content of H_2O is directly undetectable, it is defined in response to fractional conversion (f) via the relationship $R_0 = R_p(f) + R_f(1 - f)$. ^{18}O KIEs were extracted from linear regression analysis of the data depicted in Figure 3.

$$^{18}O\ KIE = \left[1 + \frac{\ln(R_f/R_0)}{\ln(1-f)}\right]^{-1} \tag{10}$$

Table 1 summarizes the ^{18}O KIEs upon water oxidation initiated by $[\mathbf{Ru^{II}OH_2}]^{2+}$. Experiments were conducted at fixed ionic strengths and by variation of the concentration of sacrificial oxidants in 0.1 and 1.0 M $HClO_4$ and HNO_3 acids (pH 0 and 1) as well as 0.05 M KPi buffer (pH 7.2). The ^{18}O KIEs are independent of the initial concentrations of the specified oxidant and ionic strengths (μ) from 0.1 to 1.3 M. The ^{18}O KIEs at pH 0 and 1 are indistinguishable despite the potential differences in Ce^{IV} speciation (vide infra). Interestingly, the ^{18}O KIEs are independent of the catalyst TONs, from 1 to 20. This behavior is consistent with the same mechanism occurring under single-turnover and multiturnover conditions.

Steady-state kinetic data were collected using a Clark-type O_2 electrode under the conditions used to determine ^{18}O KIEs. Two sets of rate constants are quoted at controlled and uncontrolled ionic strengths (k_{un} and k_{con}), as noted by μ in Table 1. The results span the range of ionic strengths used in all ^{18}O KIE measurements (μ = 0.15−1.3 M).[15] Observed rates were found to be first-order with respect to $[\mathbf{Ru^{II}OH_2}]^{2+}$ and either first- or second-order with respect to Ce^{IV}, depending upon the solution pH. These results are consistent with literature precedent implicating Ce^{IV} aggregates.[34,35] Ce^{IV} monomers are favored at pH 0, whereas Ce^{IV}−O−Ce^{IV} bridged dimers are increasingly formed at pH 1.The $E^{\circ\prime}$ values of these species appear to be indistinguishable, suggesting that the monomeric and dimeric oxidants exhibit similar reactivity.

The steady-state rate constants that depend upon the Ce^{IV} concentration and solution pH, as described above and further below, differ markedly from the more rapid pre-steady-state rate constants reported by Wasylenko et al. under single-turnover conditions.[6] The latter values, corresponding to eqs 1−6 in Figure 2, were used in the construction of the reaction coordinate diagrams. The reported k_{O_2} at pH 1 (1.9×10^{-4} s^{-1}) is within experimental error of the rate constant corresponding to decay of the $[\mathbf{Ru^{V}{=}O}]^{3+}$ intermediate to a species that absorbs at 688 nm (1.2×10^{-4} s^{-1}).[6] At pH 0, no spectroscopic signal for the 688 nm absorbing species could be detected possibly because it is consumed more rapidly than it is formed.

The steady-state kinetic parameters determined in this study reflect ET, PCET, and/or oxidant-assisted H_2O attack upon $[\mathbf{Ru^{V}{=}O}]^{3+}$ under conditions comparable to those used to determine the ^{18}O KIEs. Apparent bimolecular rate constants of ∼0.9 M^{-1} s^{-1} were observed for reactions of CAN in 1.0 M $HClO_4$ and in the presence of added $LiClO_4$. k_{un} and k_{con} are indistinguishable in 1.0 M HNO_3 and in the presence of added KNO_3, consistent with H_2O acting as the proton acceptor in the associated PCET reactions. Somewhat smaller rate constants ∼0.55 M^{-1} s^{-1} were observed for CS in 1.0 M HNO_3, as well as with added KNO_3, consistent with the in situ generation of $[Ce^{IV}(NO_3)_6]^{2-}$. Raising the pH may cause $[Ce^{IV}(NO_3)_6]^{2-}$ to dimerize to form another anionic species. Under such conditions, ionic screening could account for the increase in termolecular rate constant at pH 1 where k_{un} varies from ∼0.7 M^{-2} s^{-1}, at μ = 0.16−0.70, to k_{con} ∼ 2.3 M^{-2} s^{-1}, at μ = 1.0 M in the presence of added $LiClO_4$. The absence of an ionic strength effect is anticipated for the neutral $Ce^{IV}(SO_4)_2(H_2O)_4$ as observed. Yet, insolubility of the salt precluded comparisons at pH 0.

The largest ^{18}O KIEs, ranging from 1.0235 to 1.0312, are associated with water oxidation in different media where the oxidant's structure may be influenced by the presence of nitrate ions. These results implicate $[Ce^{IV}(NO_3)_6]^{2-}$ as a common reactant. Importantly, there is no evidence for competing side reactions, where NO_3^- is converted to NO_2 or NH_3 is converted to nitrogen oxides.[8,9,36] The formation of such volatiles could interfere with single-turnover experiments conducted at 4:1 oxidant-to-catalyst ratios, where the pressure of CO_2 indicates a 96 ± 8% yield of O_2.

The removal of impurities during the purification and subsequent combustion of O_2 notwithstanding, if CO_2 samples were contaminated by natural-abundance NO_2, the apparent ^{18}O KIE would decrease relative to the actual value. The reason is that $^{16}O{=}^{14}N{=}^{16}O$ with mass 46 would overlap with the signal for $^{16}O{=}^{12}C{=}^{18}O$, which is analyzed relative to

dx.doi.org/10.1021/ic202745n | Inorg. Chem. 2012, 51, 4722−4729

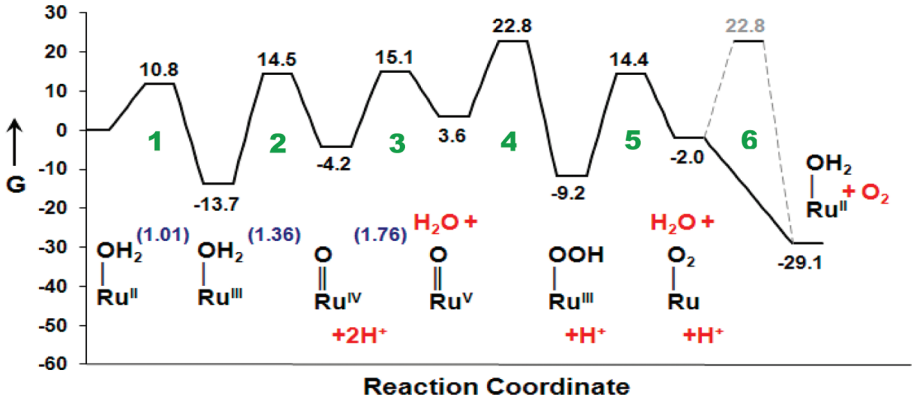

Figure 4. Reaction coordinate for ruthenium-catalyzed water oxidation by CAN in 1.0 M $HClO_4$. Only unimolecular reactions are shown, corresponding to steps 1−6 in Figure 2. All values are in kcal mol^{-1} except for $E^{\circ\prime}$, which is given in V vs NHE (in blue).

$^{16}O{=}{}^{12}C{=}{}^{16}O$ with a mass of 44 when determining the competitive ^{18}O KIE. In a different scenario, the use of ^{18}O-depleted nitrate could give rise to the ^{16}O-enriched catalyst from which production of O_2 would be characterized by a spuriously large normal ^{18}O KIE. This possibility is unlikely in view of past results,[6,8,36] including those conducted with ^{18}O-labeled water as well as ^{16}O-labeled CAN and NO_3^-, which gave $^{18,18}O_2$ as the major product, and present results that demonstrate reproducible ^{18}O KIEs upon variation of the concentration and source of nitrate. Thus, the data indicate an intrinsically larger ^{18}O KIE in the presence of $[Ce^{IV}(NO_3)_6]^{2-}$, although its coordination labile nature could make this conclusion an oversimplification. Nevertheless, the isotope effect indicates decreased barriers to ET and PCET and an increased barrier to O−O coupling along the reaction coordinate.

Catalytic water oxidation by CS in 0.1 M $HClO_4$ is characterized by an ^{18}O KIE = 1.0132. As mentioned, $Ce^{IV}(SO_4)_2(H_2O)_4$ is expected to act as the electron acceptor, while H_2O acts as the proton acceptor, considering the pK_a of H_3O^+ (−1.7) under the experimental conditions.[17] The substitution of $HClO_4$ by HNO_3 results in near doubling of the ^{18}O KIE to 1.0233, consistent with the increased involvement of $[Ce^{IV}(NO_3)_6]^{2-}$, as described above. It is unclear if the ^{18}O KIE is intrinsically smaller when H_2O attacks $[\mathbf{Ru^V{=}O}]^{3+}$ in the absence of nitrate or if this step is simply less rate-limiting. The latter would seem unlikely in view of the similar thermodynamics expected for water oxidation by CAN and CS.

A small ^{18}O KIE = 1.0141 is also observed for catalyzed water oxidation via $[Ru^{III}(bpy)_3]^{3+}$ in 0.05 M KPi at pH 7.2. Yields of O_2 varied between 4 and 12% of the $K_2S_2O_8$ initially present, and no oxidation was detectable in control experiments conducted in the absence of catalyst. As described below, the reaction is envisioned to occur by multisite PCET,[22,23] where ET to $[Ru^{III}(bpy)_3]^{3+}$ occurs concomitant with PT from the ruthenium catalyst to the hydrogen-bonded HPO_4^{2-} (pK_a 7.2). Evidence has recently been reported that bases such as HPO_4^{2-} can activate H_2O for O−O bond coupling,[13] lowering the transition-state energy by 4−5 kcal mol^{-1} relative to the reaction at low pH. The smaller ^{18}O KIE may result from base-assisted O−O bond formation, where the reaction-coordinate frequency is less isotope-sensitive because of the involvement of combined vibrational modes or a rate-limiting step that is only partially controlled by O−O coupling due to competing ET or PCET (vide infra).

DISCUSSION

The competitive ^{18}O KIE reflects all steps beginning with the initial interaction of $[\mathbf{Ru^{II}OH_2}]^{2+}$ and H_2O up to and including the first irreversible step(s). Together these reactions dictate the ratio of $^{16,16}O_2$ to $^{16,18}O_2$ produced. In the present study, ^{18}O enrichment of H_2O occurs commensurate with ^{18}O depletion of O_2. Moderate-to-large normal ^{18}O KIEs are associated with catalysis by a synthetic ruthenium complex, in marked contrast to the inverse ^{18}O KIEs associated with PSII.[26−30] As discussed at the outset, this phenomenon can been attributed to differences in the O−O bond-formation step as well as interference by O_2 reduction.

To illustrate the utility of ^{18}O KIEs as mechanistic probes, kinetic data and reduction potentials are used to formulate a Gibbs free-energy reaction coordinate diagram for catalyzed water oxidation at pH 0. The diagram in Figure 4 reflects the uphill thermodynamics of converting $[\mathbf{Ru^{II}OH_2}]^{2+}$ to $[\mathbf{Ru^V{=}O}]^{3+}$, which is primed for reaction with H_2O. Similar results were obtained at pH 1,[15] as expected based on Ce^{IV} speciation. There is evidence that Ce^{IV} dimerizes but this process does not influence the $E^{\circ\prime}$ presented in Table 1.

In the first step of Figure 4, ET occurs with $k_1 = 2.8 \times 10^5$ M^{-1} s^{-1}. The second step is nominally a PCET that converts $[Ru^{III}OH_2]^{3+}$ to $[Ru^{IV}{=}O]^{2+}$ and $2H_3O^+$ with $k_2 \sim 10^3$ M^{-1} s^{-1}. In the third step, $[Ru^{IV}{=}O]^{2+}$ is oxidized with $k_3 = 2 \times 10^2$ M^{-1} s^{-1}. These bimolecular rate constants are converted to unimolecular rate constants using electrostatic work terms and the adiabatic assumption outlined above.[15,37,38] Although the rate constant for O−O bond coupling could not be determined accurately at pH 0, a value of $k_4 = 1.2 \times 10^{-4}$ s^{-1} has been measured at pH 1 and serves here as a reasonable estimate.[6,36] Hughes and Friesner have predicted similar barriers to O−O bond formation for similar monomeric catalysts.[41] We also note that a much smaller $\Delta G^{\ddagger}$ = 1.7 kcal mol^{-1} has been proposed by Wang and Van Voorhis using four rather than two assisting H_2O molecules in the transition state for the O−O bond-forming step.[42] Water networks have been suggested to sustain "proton relays" that could cause the barrier to O−O coupling to be dominated by solvent reorganization, even in the case of a dimeric ruthenium catalyst.[43]

Intermediates subsequent to O−O bond formation have not been observed experimentally in the present system. For this reason, $\Delta G^{\ddagger}$ for $[Ru^{III}OOH]^{2+}$ oxidation is approximated using the Marcus cross-relation, by including the intrinsic barriers determined for the analogous PCET oxidation of $[Ru^{III}OH]^{2+}$

dx.doi.org/10.1021/ic202745n | Inorg. Chem. 2012, 51, 4722−4729

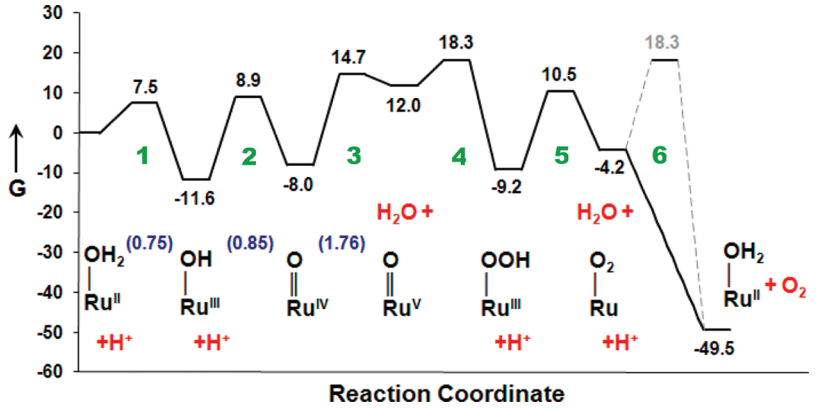

Figure 5. Reaction coordinate for ruthenium-catalyzed water oxidation by $[Ru^{III}(bpy)_3]^{3+}$ in 0.05 M KPi (pH 7.2). For simplicity, the uncomplexed catalyst is shown corresponding to steps 1−6 of Figure 2. All values are in kcal mol^{-1} except for $E^{\circ\prime}$ given in V vs NHE (in blue).

and the appropriate $\Delta G^{\circ\prime}$.[15] An apparent turnover rate constant of ~1.9 × 10^{-4} has been reported for O_2 evolution[6] at saturating levels of CAN at pH 0. The interpretation of this rate constant, determined by monitoring O_2 evolution, is still an open question; however, the value is remarkably close to k_4; this suggests that O−O coupling and O_2 release from $[RuO_2]^{2+}$ may both contribute to the turnover-limiting step.

Interestingly, the steady-state rate constants determined with CS resemble those obtained with CAN under similar experimental conditions. The changeover from first order to second order behavior is observed upon an increase in the pH from 0 to 1, while the rate constants should increase in proportion to the increased $E^{\circ\prime}$. As noted above, the one parameter that differentiates the Ce^{IV} reactions is the ^{18}O KIE. Assuming that the intrinsic barriers to ET are the same for the two oxidants, together with the indistinguishable $E^{\circ\prime}$, suggests that the reaction-coordinate diagram for CS at pH 0 should resemble that of CAN in Figure 4. Further, the smaller ^{18}O KIE observed with CS implies a unique transition-state structure where the mode corresponding to O−O bond formation is less isotopically sensitive. Thus, the results for CS in comparison to CAN raise the possibility that the Ce^{IV} reagent is directly involved in the O−O bond-forming step.[9]

As a complement to the low-pH experiments with Ce^{IV}, water oxidation at pH 7.2 (0.05 M KPi buffer) has been examined with a photogenerated source of $[Ru(bpy)_3]^{3+}$ as the oxidant. The experiments resemble those of Fecenko et al.,[22,23] where tyrosine oxidation by $[Ru(bpy)_3]^{3+}$ ($E^{\circ\prime}$ = 1.24 V) was facilitated by HPO_4^{2-} at sufficiently high concentrations. A similar model is invoked here to understand the effectiveness of multisite PCET involving the ruthenium catalyst, which is likely to be hydrogen-bonded to HPO_4^{2-}. This complex, where the proton can shuttle between donor and acceptor, interacts electrostatically with $[Ru(bpy)_3]^{3+}$ prior to ET or PCET. Although termolecular complexes of the catalyst, oxidant, and base/H_2O are believed to exist transiently in solution, only the catalyst is shown in the reaction-coordinate diagram to draw attention to its transformations.

Kinetic data are not yet available for water oxidation by photogenerated $[Ru^{III}(bpy)_3]^{3+}$ at pH 7.2. Therefore, the reaction-coordinate diagram in this case utilizes rate constants predicted using adiabatic Marcus theory.[37−39] The adiabatic approach allows comparisons of $\Delta G^{\ddagger}$ for O−O bond formation to the highest possible $\Delta G^{\ddagger}$ for PCET and ET in Figure 5. Although the latter reactions are formally nonadiabatic,[17] averaging electronic coupling and Franck−Condon overlap factors can result in successful applications of the Marcus cross-relation.[37,40]

Barriers to PCET in Figure 5 were predicted using the Marcus cross-relation. In each case, the self-exchange rate constant for $[Ru^{III}(bpy)_3]^{3+}$ + $[Ru^{II}(bpy)_3]^{2+}$ (~2 × 10^9 M^{-1} s^{-1})[21] was used together with an estimated self-exchange rate constant for one of the following reactions: $\{[Ru^{II}OH_2]^{2+}[HPO_4]^{2-}\}$ + $\{[Ru^{III}OH]^{2+}[H_2PO_4]^{-}\}$, $\{[Ru^{III}OH]^{2+}[HPO_4]^{2-}\}$ + $\{[Ru^{IV}O]^{2+}[H_2PO_4]^{-}\}$ and $\{[Ru^{III}OOH]^{2+}[HPO_4]^{2-}\}$ + $\{[RuO_2]^{2+}[H_2PO_4]^{-}\}$. Using tyrosine as a model, 4.3 × 10^{-4} M^{-1} s^{-1} is derived for multisite PCET effected by $[Ru^{III}(bpy)_3]^{3+}$ in KPi buffer.[22,23] $\Delta G^{\circ\prime}$ for each PCET step was calculated from bond-dissociation free energies, as previously described.[15,17,44] The results are rather insensitive to the estimated intrinsic barrier. For instance, increasing the value of the multisite PCET self-exchange rate constant by 12 orders of magnitude, from ~4 × 10^{-4} to 4 × 10^8 M^{-1} s^{-1}, does not impact the assignment of the rate-limiting step.

Following the first two PCET steps in Figure 5, a thermodynamically disfavored ET could compete with O−O bond coupling in the first irreversible and rate-limiting step. The barrier was calculated using the rate constant for $[Ru^{III}(bpy)_3]^{3+}$ + $[Ru^{II}(bpy)_3]^{2+}$ and an estimated self-exchange rate constant for $[Ru^{IV}{=}O]^{2+}$ + $[\mathbf{Ru^{V}{=}O}]^{3+}$ (≥2 × 10^5 M^{-1} s^{-1}), which is based upon experimental and theoretical analyses of rate constants for PCET involving structurally related molecules.[45,46] The O−O coupling step in which $[\mathbf{Ru^{V}{=}O}]^{3+}$ reacts with H_2O is the highest point on the free-energy surface, with $\Delta G^{\ddagger}$ = 18.3 kcal mol^{-1} estimated assuming the ~4.5 kcal mol^{-1} barrier-lowering effect upon replacement of H_2O with HPO_4^{2-} in neutral aqueous solution.[13] If $\Delta G^{\ddagger}$ were only 1.7 kcal mol^{-1} for O−O coupling,[42] this step would compete with the preceding ET and diminish the ^{18}O KIE (vide infra). The release of O_2 has also been considered a potential turnover-limiting step in catalysis by certain monomeric ruthenyl complexes.[10] In the present study, this reaction is thermodynamically quite downhill. Further, if O_2 release were significantly rate-limiting, an ^{18}O KIE less than or equal to unity would be expected.[24,25]

Presented below are expressions for ^{18}O KIEs upon catalyzed water oxidation at two extremes. The treatment used does not explicitly consider an ^{18}O KIE that may result from the binding of H_2O to $[\mathbf{Ru^{II}OH_2}]^{2+}$. The latter was prepared from natural-abundance reagents and pre-equilibrated before use. Attempts to observe a change from R_{H_2O} = 0.9930 ± 0.0006 upon pre-

dx.doi.org/10.1021/ic202745n | Inorg. Chem. 2012, 51, 4722−4729

incubation of water with the catalyst (and the sacrificial oxidant in separate experiments) showed no sign of change.

In eq 13, all steps in Figure 2 leading up to O−O bond formation are assumed to be kinetically reversible. Thus, each reaction, excluding irreversible O−O bond formation, should be characterized by an inverse oxygen-18 equilibrium isotope effect (^{18}O EIE) because of the net increase and strengthening of bonds in the product relative to the reactant state.[24,25] Therefore, the ^{18}O KIE is the product of three inverse ^{18}O EIEs and a normal ^{18}O KIE on the fourth irreversible step.

At the other extreme, each step is kinetically irreversible, resulting in eq 14. The observed isotope effect is therefore a weighted average of ^{18}O KIEs on all microscopic steps that contribute to rate-limitation. Here the ^{18}O KIE can only be as large as the ^{18}O KIE on the microscopic O−O bond formation. Benchmark ^{18}O KIEs of ≤1.015 have been determined for ET, while ^{18}O KIEs of ≤1.0075 have been identified with PCET reactions analogous to the ones in this study.[48,49] Contributions from ET and/or PCET to the rate-limiting step could explain the smaller ^{18}O KIEs of ∼1.013 and 1.014 observed for reactions where CS and $[Ru^{III}(bpy)_3]^{3+}$ are the oxidants. Yet, this kinetic treatment does not readily account for the reactions of CAN, where the ^{18}O KIE ∼ 1.030, or the reactions where CS is used in 1.0 M HNO_3 to produce an ^{18}O KIE ∼ 1.023.

Importantly, O_2 release is expected to have an ^{18}O KIE of ≤1.[24,25] Its contribution to the rate-limiting step would therefore reduce the maximum ^{18}O KIE substantially. While there may be multiple ways to explain the smaller ^{18}O KIEs observed in this study, there seems to be only a single way to explain ^{18}O KIEs of >1.02.[47] The latter must involve a primarily rate-limiting O−O bond-coupling step and a transition state with significant oxygen motion. Isotope effects upon the reaction-coordinate frequency terms are invariably normal and can be sizable in the reactions of interest.[25,47] Values upward of 1.02 have been reported earlier in investigations of O−O bond heterolysis, which can be visualized as the microscopic reverse of O−O bond formation by a base-assisted water attack. The discussion thus far has assumed that no significant ^{18}O EIE characterizes the ligand self-exchange where $[\mathbf{Ru^{II}OH_2}]^{2+}$ reacts with H_2O.[50] We have computationally addressed such cases and found that the ^{18}O EIE is indistinguishable from unity. We are also in the process of experimentally verifying this assumption through ^{18}O KIE measurements on reactions of the related anhydrous and chloride complexes.[51]

$$^{18}\text{O KIE} = \frac{^{18}k_1}{^{18}k_{-1}}\frac{^{18}k_2}{^{18}k_{-2}}\frac{^{18}k_3}{^{18}k_{-3}}{}^{18}k_4 \quad (13)$$

$$^{18}\text{O KIE} = \frac{w_1{}^{18}k_1 + w_2{}^{18}k_2 + w_3{}^{18}k_3 + w_4{}^{18}k_4}{w_1 + w_2 + w_3 + w_4} \quad (14)$$

CONCLUSIONS

The findings presented provide the first evidence of normal ^{18}O KIEs upon O−O bond formation during catalytic water oxidation. The largest ^{18}O KIE ∼ 1.030 observed in this study, with CAN as the oxidant in an acidic solution, is attributed to O−O bond formation in the irreversible rate-limiting step. Competing ET and PCET steps are excluded because of the lower estimated free-energy barriers and the much smaller expected ^{18}O KIEs. In addition, the ^{18}O EIEs accompanying all ET and PCET steps are inverse. If such steps were to occur reversibly prior to O−O bond formation, the ^{18}O KIE on this microscopic step would have to be even larger than the observed value of ∼1.03. Although we cannot rigorously exclude O_2 release in the turnover-controlling step, this reaction is expected to have an ^{18}O KIE of ≤1 based upon numerous experimental and computational findings.[24] In addition, the downhill thermodynamics after the O−O bond is formed makes hydroperoxo intermediate oxidation and O_2 release poor candidates for the turnover-controlling step.

The results further suggest that ^{18}O KIEs upon O−O bond formation are susceptible to subtle variations in the transition-state structure. Although it is conceivable that the rate-limiting step changes upon substitution of CAN by ceric sulfate, the kinetics and thermodynamics are essentially unchanged. It follows that the significantly diminished ^{18}O KIE ∼ 1.013 could reflect a unique transition state, wherein the oxidant has a crucial role. Because $Ce^{IV}(SO_4)_2(H_2O)_4$ lacks the polarizing influence of $[Ce^{IV}(NO_3)_6]^{2-}$, different transition states involving ordered H_2O molecules may be anticipated. Catalyzed water oxidation by $[Ru^{III}(bpy)_3]^{3+}$ in neutral aqueous solutions containing 0.05 M HPO_4^{2-} also exhibits a small ^{18}O KIE ∼ 1.014. The reason for this may again be variation in the transition-state structure in the presence of an activating base; however, the unfavorable thermodynamics of forming the reactive $[\mathbf{Ru^V{=}O}]^{3+}$ could make this the rate-limiting step.

Density functional theory (DFT) calculations are presently underway to address how H_2O might be activated for oxidation. The aggregate data obtained thus far suggest that the amplitude of O−O motion in the transition state controls the size of the ^{18}O KIE. This proposal is consistent with an earlier study of O−O bond heterolysis, which revealed a large isotope effect (∼1.02) on the imaginary mode defining the transition state. As a result, the isotopically sensitive reaction-coordinate frequency could make the ^{18}O KIE large and normal in the directions of both bond making and bond breaking. Conversely, if the transition state were dominated by solvent reorganization to accommodate a "proton relay", the ^{18}O KIE should be negligible. For the reasons above, the integration of theory and experiment promises to have a crucial role in illuminating mechanisms of water oxidation catalysis.

ASSOCIATED CONTENT

Supporting Information

Derivations, kinetic data, and complex characterization. This material is available free of charge via the Internet at http://pubs.acs.org.

AUTHOR INFORMATION

Corresponding Author

*E-mail: jproth@jhu.edu.

Notes

The authors declare no competing financial interest.

ACKNOWLEDGMENTS

We are grateful for support from the DOE Basic Energy Sciences (Grant DE-FG02-09ER16094) and ACS-PRF (Grant 50046ND3). We also wish to thank Ben Passey, Eric Sun, Chris Cramer, and Zahid Ertim for technical assistance and insightful discussions.

REFERENCES

(1) Bockris, J. O'M. *Int. J. Hydrogen Energy* **2002**, *27*, 731.

(2) Lewis, N. S.; Nocera, D. G. *Proc. Natl. Acad. Sci. U.S.A.* **2006**, *103*, 15729.
(3) Concepcion, J. J.; Jurss, J. W.; Brennaman, M. K.; Hoertz, P. G.; Patrocinio, M. K. O.; Iha, N. Y. M.; Templeton, J. L.; Meyer, T. J. *Acc. Chem. Res.* **2009**, *42*, 1954.
(4) Concepcion, J. J.; Tsai, M.-K.; Muckerman, J. T.; Meyer, T. J. *J. Am. Chem. Soc.* **2010**, *132*, 1545.
(5) Wasylenko, D. J.; Ganesamoorthy, C.; Koivisto, B. D.; Henderson, M. A.; Osthoff, H. D.; Berlinguette, C. P. *J. Am. Chem. Soc.* **2010**, *132*, 16094.
(6) Wasylenko, D. J.; Ganesamoorthy, C.; Henderson, M. A.; Berlinguette, C. P. *Inorg. Chem.* **2011**, *50*, 3622.
(7) Wasylenko, D. J.; Ganesamoorthy, C.; Koivisto, B. D.; Henderson, M. A.; Berlinguette, C. P. *Inorg. Chem.* **2010**, *29*, 2202.
(8) Masaoka, S.; Sakai, K. *Chem. Lett.* **2009**, *38*, 182.
(9) Kimoto, A.; Yamauchi, K.; Yoshida, M.; Masaoka, S.; Sakai, K. *Chem. Commun.* **2012**, *48*, 239.
(10) Polyansky, D. E.; Muckerman, J. T.; Rochford, J.; Zong, R.; Thummel, R. P.; Fujita, E. *J. Am. Chem. Soc.* **2011**, *133*, 14649.
(11) Takeuchi, K. J.; Thompson, M. S.; Pipes, D. W.; Meyer, T. J. *Inorg. Chem.* **1984**, *23*, 1845.
(12) Concepcion, J. J.; Jurss, J. J.; Templeton, J. L.; Meyer, T. J. *J. Am. Chem. Soc.* **2008**, *130*, 16462.
(13) Chen, Z.; Concepcion, J. J.; Hu, Q.; Yang, W.; Hoertz, P. G.; Meyer, T. J. *Proc. Natl. Acad. Sci. U.S.A.* **2010**, *107*, 7225.
(14) Rapaport, I.; Helm, L.; Merbach, A. E.; Bernhard, P.; Ludi, A. *Inorg. Chem.* **1988**, *28*, 873.
(15) See the Supporting Information.
(16) (a) Roth, J. P. *Physical Inorganic Chemistry: Methods and Techniques*; Wiley: New York, 2010; Vol. *1*, pp 425−457. (b) Smirnov, V. V.; Brinkley, D. W.; Lanci, M. P.; Karlin, K. D.; Roth, J. P. *J. Mol. Catal. A* **2006**, *251*, 100.
(17) Huynh, M. H. V.; Meyer, T. J. *Chem. Rev.* **2007**, *107*, 5004.
(18) (a) Cape, J. L.; Siems, F.; Hurst, J. K. *Inorg. Chem.* **2009**, *48*, 9729. (b) Brunschwig, B. S.; Chou, M. H.; Creutz, C.; Ghosh, P.; Sutin, N. *J. Am. Chem. Soc.* **1983**, *105*, 4833.
(19) Binnemans, K. In *Handbook on Physics and Chemistry of Rare Earths*; Gschneidner, K. A., Jr.; Bünzli, J.-C. G.; Pacharsky, V. K., Eds.; Elsevier, London, 2006; Vol. *36*.
(20) Yee, E. L.; Hupp, J. T.; Weaver, M. J. *Inorg. Chem.* **1983**, *22*, 3465.
(21) Young, R. C.; Keene, F. R.; Meyer, T. J. *J. Am. Chem. Soc.* **1977**, *99*, 2468.
(22) Fecenko, C. J.; Meyer, T. J.; Thorp, H. H. *J. Am. Chem. Soc.* **2006**, *128*, 11020.
(23) Fecenko, C. J.; Meyer, T. J.; Thorp, H. H. *J. Am. Chem. Soc.* **2007**, *49*, 15099.
(24) Roth, J. P. *Acc. Chem. Res.* **2009**, *42*, 399.
(25) Ashley, D. C.; Brinkley, D. W.; Roth, J. P. *Inorg. Chem.* **2010**, *49*, 3661.
(26) Tcherkez, G.; Farquhar, G. D. *Funct. Plant Biol.* **2007**, *34*, 1049.
(27) Eisenstadt, D.; Barkan, E.; Luz, B.; Kaplan, A. *Photosynth. Res.* **2010**, *103*, 97.
(28) Burda, K.; Bader, K. P.; Schmid, G. H. *Biochim. Biophys. Acta* **2003**, *1557*, 77.
(29) Metzner, H.; Fischer, K.; Bazlen, O. *Biochim. Biophys. Acta Bioenerg.* **1979**, *548*, 287.
(30) Guy, R. D.; Fogel, M. L.; Berry, J. A. *Plant Physiol.* **1993**, *101*, 37.
(31) Epstein, S.; Mayeda, T. *Geochim. Cosmochim. Acta* **1953**, *4*, 213.
(32) Coplen, T. B. *Nature* **1995**, *375*, 285.
(33) O'Leary, M. H. *Phytochemistry* **1981**, *20*, 553.
(34) Yu, P.; O'Keefe, T. J. *J. Electrochem. Soc.* **2006**, *153*, C80.
(35) Duke, F. R.; Parchen, F. R. *J. Am. Chem. Soc.* **1956**, *78*, 1540.
(36) Moyer, B. A.; Meyer, T. J. *J. Am. Chem. Soc.* **1979**, *101*, 1326.
(37) Marcus, R. A.; Sutin, N. *Biochim. Biophys. Acta* **1985**, *811*, 265.
(38) If this rate constant were somehow misinterpreted or elevated by a few orders of magnitude, the barrier to O−O bond formation ($\Delta G^{\ddagger}$ = ∼18 kcal mol^{-1}) would still represent the highest along the reaction coordinate, most importantly exceeding those barriers associated with ET and PCET steps.
(39) The Marcus cross-relation is a corollary of the basic Marcus equation: $\Delta G^{\ddagger} = \lambda/4(1 + \Delta G^{\circ\prime}/\lambda)$, where λ is the average of two self-exchange reactions. Although probabilistic effects associated with electron and proton tunneling are unaccounted for, the adiabatic approximation gives the upper bounds to $\Delta G^{\ddagger}$ based upon the expression k_{ET} or $k_{PCET} = \kappa k_B T/h \exp^{-\Delta G^{\ddagger}/RT}$, where k_B and h are Boltzmann's and Planck's constants, T is the temperature, and κ, the transmission coefficient, is assumed to be unity, causing the preexponential term to approach the frequency of a bond vibration (∼10^{13} s^{-1}). Although bimolecular rate constants are measured, electrostatic work corrections are included to make these unimolecular rate constants, as described in ref 37; i.e., $\Delta G_{uni}^{\ddagger} = \Delta G_{bi}^{\ddagger} + w_R$. Work terms are also used to compute the Gibbs free energies ($\Delta G^{\circ\prime} = \Delta G^{\circ} + w_P - w_R$), as detailed in the Supporting Information.
(40) Roth, J. P.; Yoder, J. C.; Wan, T.-J.; Mayer, J. M. *Science* **2001**, *294*, 2524.
(41) Hughes, T. F.; Friesner, R. A. *J. Phys. Chem.* **2011**, *115*, 9280.
(42) Wang, L.-P.; Van Voorhis, T. *Inorg. Chem.* **2010**, *49*, 4543.
(43) Bianco, R.; Hay, P. J.; Hynes, J. T. *J. Phys. Chem. A* **2011**, *115*, 8003.
(44) Warren, J. J.; Tronic, T. A.; Mayer, J. M. *Chem. Rev.* **2010**, *110*, 6961.
(45) (a) Farrer, B. T.; Thorp, H. H. *Inorg. Chem.* **1999**, *38*, 2497. (b) Binstead, R. A, Meyer, T. J. 1987, *109*, 3287.
(46) Iordanova, N.; Hammes-Schiffer, S. *J. Am. Chem. Soc.* **2002**, *124*, 4848.
(47) Roth, J. P.; Cramer, C. J. *J. Am. Chem. Soc.* **2008**, *130*, 7802.
(48) (a) Buhks, E.; Bixon, M.; Jortner, J. *J. Phys. Chem.* **1981**, *85*, 3763. (b) Guarr, T.; Buhks, E.; McLendon, G. *J. Am. Chem. Soc.* **1983**, *105*, 3763.
(49) Huff, G. S.; Doncheva, I. S.; Brinkley, D. W.; Angeles-Boza, A. M.; Mukherjee, A.; Cramer, C. J.; Roth, J. P. *Biochemistry* **2011**, *50*, 7375.
(50) A related type of reaction is described in: Rutenburg, A. C.; Taube, H. *J. Chem. Phys.* **1952**, *20*, 825.
(51) This result does not necessarily contradict the works of Taube, who seemed to have measured an equilibrium isotope effect beginning with the labeled metal complex and unlabeled H_2O. At the time, the reverse reaction was not considered. When reagents are present at natural-abundance levels, ^{18}O EIE = $w_1(^{16,16}K/^{16,18}K) + w_2(^{16,16}K/^{18,16}K)$, with the weighting factors (w_1 and w_2) representing asymmetric reactions. These factors are typically similar but can differ due to energy differences of the DFT-optimized structures.